Antiviral Research 91 (2011) 1–10

Contents lists available at ScienceDirect

Antiviral Research

journal homepage: www.elsevier.com/locate/antiviral

Interference of ribosomal frameshifting by antisense peptide nucleic acids suppresses SARS coronavirus replication

Dae-Gyun Ahn [a], Wooseong Lee [a], Jin-Kyu Choi [a], Seong-Jun Kim [a], Ewan P. Plant [b], Fernando Almazán [c], Deborah R. Taylor [b], Luis Enjuanes [c], Jong-Won Oh [a,*]

[a] Department of Biotechnology and Translational Research Center for Protein Function Control, Yonsei University, Seoul 120-749, Republic of Korea
[b] Laboratory of Hepatitis and Related Emerging Agents, Division of Emerging and Transfusion Transmitted Diseases, Office of Blood Research and Review, Center for Biologics Evaluation and Research, Food and Drug Administration, Bethesda, MD, USA
[c] Department of Cell and Molecular Biology, Centro Nacional de Biotecnología, CSIC, Campus Universidad Autónoma, Cantoblanco, C/Darwin 3, 28049 Madrid, Spain

ARTICLE INFO

Article history:
Received 17 November 2010
Revised 9 March 2011
Accepted 19 April 2011
Available online 23 April 2011

Keywords:
SARS-CoV
Frameshifting
Peptide nucleic acids
RNA replication

ABSTRACT

The programmed −1 ribosomal frameshifting (−1 PRF) utilized by eukaryotic RNA viruses plays a crucial role for the controlled, limited synthesis of viral RNA replicase polyproteins required for genome replication. The viral RNA replicase polyproteins of severe acute respiratory syndrome coronavirus (SARS-CoV) are encoded by the two overlapping open reading frames 1a and 1b, which are connected by a −1 PRF signal. We evaluated the antiviral effects of antisense peptide nucleic acids (PNAs) targeting a highly conserved RNA sequence on the – PRF signal. The ribosomal frameshifting was inhibited by the PNA, which bound sequence-specifically a pseudoknot structure in the −1 PRF signal, in cell lines as assessed using a dual luciferase-based reporter plasmid containing the −1 PRF signal. Treatment of cells, which were transfected with a SARS-CoV-replicon expressing firefly luciferase, with the PNA fused to a cell-penetrating peptide (CPP) resulted in suppression of the replication of the SARS-CoV replicon, with a 50% inhibitory concentration of 4.4 μM. There was no induction of type I interferon responses by PNA treatment, suggesting that the effect of PNA is not due to innate immune responses. Our results demonstrate that −1 PRF, critical for SARS-CoV viral replication, can be inhibited by CPP-PNA, providing an effective antisense strategy for blocking −1 PRF signals.

1. Introduction

Severe acute respiratory syndrome coronavirus (SARS-CoV) emerged in the Guangdong province of China in November 2002 and spread to more than 30 countries worldwide, resulting in approximately 800 deaths during the SARS outbreak of 2003 (Peiris et al., 2004). Except for several suspected SARS cases, additional infection has not been reported since April 2004. However, re-emergence is a possibility due to the identification of putative natural reservoirs (Wang et al., 2006). Therefore, in the absence of specific, effective antiviral drugs for this newly emergent disease, there is a need for the development of therapeutics against SARS-CoV to control re-emergence (Cinatl et al., 2005; Tong, 2009).

The genome of SARS-CoV consists of a single-stranded, plus-sense RNA approximately 30 kb in length (Marra et al., 2003; Rota et al., 2003; Thiel et al., 2003). The large SARS-CoV RNA genome produces eight 3′-co-terminal, nested subgenomic mRNAs (sg-mRNAs) for the efficient translation of structural and accessory proteins (Masters, 2006; Snijder et al., 2003). The 5′ two-thirds of the SARS-CoV genome encode two large replicase polyproteins, expressed by open reading frames (ORF) 1a and 1b. As in other coronaviruses, ORF1a and ORF1b are slightly overlapped and, because ORF1b lacks its own translation initiation sites, the proteins encoded by ORF1b are only translated as a fusion protein together with ORF1a by programmed −1 ribosomal frameshifting (−1 PRF), (Baranov et al., 2005; Brierley et al., 1989; Plant et al., 2005; Su et al., 2005). The ORF1a and ORF1a/1b fusion proteins are proteolytically cleaved into 16 mature nonstructural proteins (nsps) that play multiple crucial roles during viral genome replication (Masters, 2006). The −1 PRF is thought to be essential for CoV genome replication because the coronavirus RNA-dependent RNA polymerase (RdRp), the key component of the replicase required for viral genome replication (Xu et al., 2003; Almazan et al., 2006; Prentice et al., 2004; te Velthuis et al., 2010), is the first part of the ORF1a/1b protein synthesized after frameshifting.

Natural ribosomal frameshifting hardly occurs during translation. However, PRF, occurring by specific signals, increases the possibility of tRNA slippage up to 50% (Baranov et al., 2002; Namy et al., 2004). The ribosomal frameshift signal consists of two

* Corresponding author. Tel.: +82 2 2123 2881; fax: +82 2 362 7265.
E-mail address: jwoh@yonsei.ac.kr (J.-W. Oh).

0166-3542/$ - see front matter © 2011 Elsevier B.V. All rights reserved.
doi:10.1016/j.antiviral.2011.04.009

elements, a heptanucleotide slippery site and a downstream tertiary RNA structure in the form of an RNA pseudoknot. SARS-CoV initiates −1 frameshifting at the three-helix-containing RNA pseudoknot (Baranov et al., 2005; Plant et al., 2005; Su et al., 2005). Recently, control of −1 PRF efficiency has been shown to be critical for the maintenance of correct stoichiometric ratios of viral replicase proteins (Plant et al., 2010). The −1 PRF signal is conserved in sequence and structure, which may constrain the ability of SASR-CoV to develop drug resistant mutants, making it an attractive target for antiviral drug discovery.

Antisense peptide nucleic acids (PNAs) have high hybridization affinity due to their neutral backbones. PNAs also exhibit superior stability compared with other anti-sense agents due to nuclease resistant properties resulting from the replacement of the deoxyribose phosphate backbone with a polypeptide backbone (Nielsen, 2010; Nielsen et al., 1991). In this study, we designed PNAs that target the pseudoknot structure of the SARS-CoV frameshifting signal, and tested the ability of these molecules to inhibit −1 PRF and SARS-CoV replication using a SARS-CoV replicon expressing a luciferase reporter.

2. Materials and methods

2.1. Cell culture and transfection

Vero and BHK-21 cells were cultured in Dulbecco's modified Eagle's medium (DMEM; BioWhittaker) supplemented with 10% fetal bovine serum (FBS; BioWhittaker), 1 mM sodium pyruvate, 100 U/ml penicillin, and 100 μg/ml streptomycin at 37 °C in a humidified atmosphere of 5% CO_2. Human embryonic kidney 293 (HEK293) cells were cultivated in DMEM supplemented with 10% FBS and penicillin/streptomycin. Vero cells grown in a 24-well plate were transfected with 0.5 μg pJD464 or pJD502 plasmids using Fugene 6 (Roche Applied Science) or DMRIE-C (Invitrogen) transfection reagents. For transfection of BHK-21 with a SARS-CoV replicon plasmid, cells (2.5×10^6) in 400 μl Opti-MEM I reduced-serum medium (Gibco BRL) were electroporated with SARS-CoV replicon plasmids (16 μg) at 260 V and 950 μF in a 4 mm electrode gap cuvette (Bio-Rad Laboratories) using a Gene Pulser II electroporator (Bio-Rad Laboratories). After electroporation, cells were incubated at room temperature for 5 min, resuspended in pre-warmed complete DMEM, and then split into 4 wells of a 6-well plate. HEK293 cells (5×10^4) were seeded in 0.5 ml medium in each well of a 48-well plate and grown overnight. Cells were then co-transfected with pSARS-REP-Feo plasmid (0.5 μg) expressing firefly luciferase and pRL-TK reporter (0.1 μg, Promega) expressing *Renilla* luciferase, with an internal control using Fugene HD transfection reagent (Roche Applied Science). After 6 h, cells were washed with serum-free medium and treated with various concentrations of PNAs in serum-free DMEM for 3 h. After washing, cells were incubated in complete medium containing 10% FBS.

2.2. Plasmids and DNA templates for in vitro transcription

pJD464 and pJD502 reporter plasmids (Plant et al., 2005), used for ribosomal frameshifting assays, have been described. pZS2 (Zhu et al., 2003), harboring the hepatitis C virus (HCV) subgenomic replicon cDNA, was used as a template for PCR-amplification of DNA template used for *in vitro* preparation of HCV 3′-untranslated region (UTR) RNA transcripts as described previously (Oh et al., 1999). To make a SARS-CoV replicon expressing a luciferase reporter from sg-mRNA, the Feo gene (Tanabe et al., 2004), comprising firefly luciferase and neomycin phosphotransferase, was fused to the transcription-regulating sequence 9 (TRS9) (Sola et al., 2005) required for synthesis of sg-mRNA9 of SARS-CoV. The TRS9 region was amplified from pBAC-SARS-CoV-REP plasmid (Almazan et al., 2006) using the forward primer MluI_F 5′-ACGCGTGGTGGTG CGCTTATAGCTAG-3′ (*Mlu*I site underlined) and the reverse primer TRS-R 5′-CTTTATGTTTTTGGCGTCTTCCATTTTAATTTGTTCGTTTATTT AAAAC-3′ (complimentary sequences to TRS9 underlined). The Feo gene was amplified from HCV replicon pRep-Feo (Tanabe et al., 2004) using the forward primer TRS-F 5′-GTTTTAAATAAAC GAACAAATTAAAATGGAAGACGCCAAAAACATAAAG-3′ (TRS9 sequences underlined) and the reverse primer BamHI-R 5′-GG ATCCTAGAAGAACTCGTCAAGAAG-3′ (*Bam*HI site underlined). The amplified TRS9 region was fused to the 5′-end of the Feo gene by bridge PCR using MluI_F and BamHI_R primers, and the resulting PCR products were inserted into the pCR2.1-TOPO vector (Invitrogen). The inserted fragment, prepared by digestion of the resulting plasmid with *Mlu*I and *Bam*HI, was then subcloned into the pBAC-SARS-CoV-REP plasmid digested with *Asc*I and *Bam*HI to make the pSARS-REP-Feo plasmid. For construction of a replication-deficient replicon control plasmid, the *Mlu*I-digested fragment from the replicase-coding gene was inserted in the reverse orientation into the pSARS-REP-Feo, to obtain pSARS-REP-Feo-MluIrev. For construction of another control plasmid, pSARS-REP-ΔTRSFeo, which lacks the TRS9, the forward primer 5′-ATTTAGAGA CGTACTTGTTGTTT TAATGGAAGACGCCAAAAACATAAAG-3′ and the reverse primer 5′-CTTTATGTTTTTGGCGTCTTCCATTAAAACAACAAGTACGTCTCTAA AT-3′ were used to amplify a DNA fragment lacking the TRS9 region. All replicon plasmids were amplified in the *Escherichia coli* strain, EPI300 (EPICENTRE Biotechnologies). *E. coli* cells were transformed in electroporation cuvettes (1 mm electrode gap) using a Gene Pulser II electroporator (Bio-Rad Laboratories) at 1.8 kV, 200 Ω, and 25 μF. Replicon plasmids were isolated using the BAC isolation kit (EPICENTRE Biotechnologies) and further purified by cesium chloride density gradient centrifugation. Replication of the SARS-CoV replicon in mammalian cells was assessed by real-time qRT-PCR, as described below, and expression of SARS-CoV capsid N protein was confirmed by Western blot analysis with anti-SARS-CoV N protein antibody (Abcam). For preparation of the −1 PRF probe, cDNA corresponding to the −1 PRF signal was synthesized by reverse transcription using the reverse primer 5′-AAAAGCCCTGTAGACGACAT-3′, complementary to nucleotides (nts) 13,456–13,475 of SARS-CoV genome. DNA templates used for *in vitro* transcription were amplified with the forward primer 5′-TAATACGACTCACTATA***GG***TTTAAACGGGTTTGCGGTGT-3′ (The T7 promoter sequence is underlined and the extra sequences added for efficient transcription by T7 RNA polymerase are shown in bold face italic), annealing to nts 13,392–13,411 of SARS-CoV genome, and the reverse primer used for cDNA synthesis.

2.3. Design of peptide nucleic acids targeting SARS-CoV −1 PRF signal

PNAs were designed to be complementary to a highly conserved SARS-CoV −1 PRF signal. Target sequences were screened by BLAST search against known human mRNA sequences to preclude unexpected gene-silencing effects. For efficient cellular uptake, PNAs were covalently linked to HIV-1 Tat peptide $Tat_{57–49}$ (RRRQRRKKR) (Wender et al., 2000) via an O-linker (AEEA, 8-amino-3,5-dioxo-octanoic acid). PNAs were obtained from Panagene Inc. (Daejeon, Korea), and sequences are listed in Table 1.

2.4. Electrophoretic mobility shift assay

PCR products containing the cDNA for −1 PRF signal were purified from a 2% agarose gel and used directly for *in vitro* transcription using the T7 MEGAscript kit (Ambion), as described previously (Yoo et al., 2009). *In vitro* transcribed RNAs were dephosphorylated with calf intestinal alkaline phosphatase

Table 1
PNAs used in this study.

Name	N-terminal CPP	Sequence (5′ → 3′)[a]	Target region[b]
Tat-UpFS	H-RRRQRRKKR	GGGTTCGCGGAGTTG	13,348–13,363
UpFS	–	GGGTTCGCGGAGTTG	13,348–13,363
Tat-FS	H-RRRQRRKKR	AGCCCTGTAGACGAC	13,458–13,472
FS	–	AGCCCTGTAGACGAC	13,458–13,472
Tat-FSm2	H-RRRQRRKKR	AGCCCT**C**TA**C**ACGAC	13,458–13,472
FSm2	–	AGCCCT**C**TA**C**ACGAC	13,458–13,472
Tat-HCV	H-RRRQRRKKR	TAAGATGGAGCCACC	9508–9522
HCV	–	TAAGATGGAGCCACC	9508–9522
Tat-J3U2	H-RRRQRRKKR	TCGGCGCTCTGTGCC	10,928–10,942

[a] PNAs are listed from N- to C-terminus, which correspond to the 5′- and 3′-terminus in nucleic acids, respectively. Underlined and boldface letters indicate mismatched bases.
[b] The nucleotide number of target regions corresponds to the published SARS-CoV genome (GenBank: AY278741), HCV genome (GenBank: AJ238799), and JEV genome (GenBank: NC_001437).

(Takara), subsequently end-labeled with [γ-^{32}P]ATP (IZOTOP) using T4 polynucleotide kinase (Takara), and purified, as described previously (Yoo et al., 2009). ^{32}P-labeled RNA probe (10 fmol) was incubated with PNAs in a total volume of 8 μl binding buffer (50 mM Tris–HCl pH 7.4, 100 mM NaCl, 1 mM DTT, 0.5% BSA) for 30 min at room temperature. After incubation, 2 μl non-denaturing loading buffer (50% glycerol, 0.02% each xylene cyanol and bromophenol blue) was added to the reaction mixtures, which were then resolved on a 5% non-denaturing polyacrylamide gel, in 1× Tris–borate–EDTA buffer (45 mM Tris base, 445 mM H_3BO_3, 1 mM EDTA) at a constant voltage of 120 V at 4 °C. After electrophoresis, the gel was dried and exposed to X-ray film for autoradiography.

2.5. Cell-based frameshift reporter assay

Vero cells (8×10^4) plated onto each well of 24-well plates were treated with various concentrations of PNAs in serum-free DMEM for 6 h. Cells were then washed with medium and transfected with 0.5 μg pJD464 or pJD502 plasmids. After 24 h, cells were harvested and lysed in lysis buffer (100 mM Tris–HCl pH 8.0, 1% Triton X-100, 150 mM NaCl) containing EDTA-free protease inhibitor cocktail (Roche Applied Science). Efficiency of ribosomal frameshifting was evaluated by dual luciferase assays using cell lysates, as described previously (Plant et al., 2005).

2.6. Real-time quantitative RT-PCR

Total RNAs were isolated using TRIzol (Invitrogen). The copy number of sg-mRNA of the SARS-CoV nucleocapsid gene was estimated by quantitative real-time reverse transcription PCR (qRT-PCR). The qRT-PCR was performed using the iQ Supermix qRT-PCR kit (Bio-Rad Laboratories) and the fluorescence was detected by CHROMO4 Continuous Fluorescence Detector (Bio-Rad Laboratories). cDNAs were synthesized using ImProm-II reverse transcriptase (Promega) and the reverse primer 5′-CGTCGGGTAG CTCTTCGGTAG-3′, complementary to nts 28,380–28,400 of the SARS-CoV genome, representing part of the nucleocapsid-coding gene. Real-time PCR was performed with the forward primer 5′-ATATTAGGTTTTTACCTACCCAGG-3′, corresponding to nucleotides 1–24 of the SARS-CoV genome, and the reverse primer used for cDNA synthesis along with a TaqMan probe [5′-6-FAM(6-carboxyfluorescein)-TCCTCCTTGCCATGCTGAGTGAGA-BHQ_1 (Black Hole Quencher 1)-3′] (Pharmatech., Inc., Korea) spanning nts 28,287–28,310 on the SARS-CoV nucleocapsid-coding region. The PCR mixture was incubated for 50 cycles of 15 s at 95 °C and 40 s at 60 °C. Standard RNA was prepared by *in vitro* transcription of PCR products amplified by the forward primer 5′-TAATACGACTCAC TATA***GGCCA***ATATTAGGTTTTTACCTACCCAGG-3′ (The T7 promoter sequence is underlined and the extra sequences added for efficient transcription by T7 RNA polymerase are shown in bold face italic) and the reverse primer used for qRT-PCR. The cDNA synthesized using the reverse primer was amplified by PCR with a short extension time (30 s at 95 °C, 30 s at 60 °C, and 30 s at 72 °C) to obtain the most abundant ∼350-bp DNA fragment representing the 5′-end region of the sg-mRNA of the N-gene. The PCR product was gel-purified, cloned, and sequenced to confirm the amplified gene. Standard RNA transcripts were purified by denaturing polyacrylamide gel electrophoresis, as described previously (Kim et al., 2004). The sg-mRNA containing the Feo gene was detected by RT-PCR using the forward primer used for real-time PCR and the reverse primer 5′-GCTTCTGCCAACCGAACGGAC-3′, complementary to a 5′-terminal region sequence of the Feo gene. The cDNA was amplified by 40 cycles (15 s at 95 °C, 30 s at 60 °C, and 30 s at 72 °C) of PCR.

qRT-PCR analysis of IFN-β and IFN-stimulated gene 56 (ISG56) transcripts was performed using SYBR Premix ExTaq (Takara) and specific oligonucleotide primers for target sequences, as well as the glyceraldehyde 3-phosphate dehydrogenase (GAPDH) housekeeping gene. The following primers were used: IFN-β: sense 5′-GAACTTTGACATCCCTGAGGAGATTAAGCAGC-3′, antisense 5′-GT CCTTAGGATTTCCACTCTGACTATGGTCC-3′; ISG56: sense 5′-TAGCCA ACATGTCCTCACAGAC-3′, antisense 5′-TCTTCTACCACTGGTTTCATG C-3′; GAPDH: sense 5′-GAAGGTGAAGGTCGGAGTC-3′, antisense 5′-GAAGATGGTGATGGGATTTC-3′ as described previously (Li et al., 2005; McCormick et al., 2004). Target gene levels normalized to GAPDH were determined using the $\Delta\Delta C_t$ method (Schmittgen and Livak, 2008).

2.7. SARS-CoV replicon replication assay

HEK293 cells transfected with pSARS-REP-Feo and pRL-TK reporter were lysed at 30 h post-transfection in 1× Glo lysis buffer (Promega) for 10 min with shaking at room temperature. Luminescence was detected using a Dual-Glo luciferase assay system (Promega) and a Glomax Multi-detection system (Promega). The relative luciferase activity was calculated by normalizing the firefly luciferase activity to the *Renilla* luciferase activity. The half maximal inhibitory concentration (IC_{50}) value was determined by fitting data to the sigmoidal equation using Sigma Plot program (SPSS Science). Human interferon (IFN)-β (Pestka Biomedical Laboratories) was used as a control for comparison with the antiviral activity of PNAs.

2.8. Cell viability

Cytotoxicity of PNAs was measured using MTT [3-(4,5-dimethylthiazol-2-yl)-2,5-diphenyl tetrazolium bromide] reagent. Vero cells grown on a 96-well plate to 70% confluence were treated with increasing concentrations of PNA in serum-free medium for 6 h. After washing, cells were incubated for 48 h in complete DMEM. Cells were stained with MTT solution (2 mg/ml) as described previously (Yoo et al., 2009), and the optical density was read on a 96-well microplate reader (FLUOstar OPTIMA, BMG Lab Technologies). Results are expressed relative to the optical density of a well containing untreated cells, defined as 100% viability. Assays were performed in triplicate.

2.9. Interferon β reporter assay

IFNβ-pGL3 luciferase reporter and the plasmid expressing a constitutively active IRF3, IRF-3(5D), were kindly provided by John Hiscott (McGill University, Montreal, Quebec, Canada) (Lin et al., 2000). HEK293 cells (5×10^4) were seeded in each well of a 48-well plate, grown overnight, and co-transfected with IFNβ-pGL3 reporter plasmid (100 ng), expressing firefly luciferase, and

pRL-TK reporter (20 ng, Promega), expressing *Renilla* luciferase used as an internal control, using Fugene HD transfection reagent (Roche Applied Science). After 6 h, cells were treated with 10 μM PNAs in serum-free DMEM for 3 h, followed by 30 h incubation in complete medium before measurement of luciferase activity by the GloMax Multi-detection system (Promega). When RNA molecules were used to induce type I IFN responses, poly inosinic:polycytidylic acid [poly(I:C), Sigma] and HCV 3′-UTR transcripts containing 5′ terminal triphosphate and poly-U/UC region were transfected into HEK293 cells using lipofectamine RNAiMax (Invitrogen) at 6 h after transfection of luciferase-reporter plasmids. At 30 h post-transfection, cells were harvested and the luminescence was measured as described above.

3. Results

3.1. Design of PNAs targeting the programmed −1 frameshift signal of the SARS-CoV genome

During translation of the SARS-CoV genome, the −1 PRF initiates at the pseudoknot RNA structure located downstream of the slippery sequence (Baranov et al., 2005; Plant et al., 2005). The pseudoknot structure is composed of three stems (S1, S2, and S3) and three loops (L1, L2, and L3) (Fig. 1A). To select PNA target sites, we initially designed various 15-mer PNAs targeting the −1 PRF signal spanning nts 13,392–13,472 by moving their target sites 1 nt towards the 3′-end of this region. All putative PNA target sequences were screened by BLAST to exclude sequences homologous to known human mRNAs. Finally, we were able to choose a single PNA, named FS PNA, targeting the region spanning nts 13,458–13,472 for analysis of its inhibitory function in −1 PRF event. No human genome sequences homologous to this target were identified by BLAST search. The selected target site, encompassing the stem 2, loop 3, and a partial region of stem 3, was highly conserved in sequence; among more than 130 strains of SARS-CoV, only one strain had a single nucleotide variation at nt-13,470 (G → A; GenBank Accession No. AY313906).

The structure of the SARS-CoV frameshift signal is extremely stable, with a minimal free energy of −26.68 kcal/mol (Plant et al., 2005). To test whether the designed PNA can invade the stable pseudoknot structure and anneal to the target, we performed electrophoretic mobility shift assays (EMSA). As shown in Fig. 1B, most of FS PNA formed a complex at a probe-to-PNA molar ratio of 1:5 (lane 3). In contrast, HCV PNA, targeting hepatitis C virus X-RNA at the 3′-UTR of the viral genome, did not form a complex even at a higher concentration of PNA (lane 5). The FSm2 PNA, in which two guanosine residues (complementary to nt 13,463 and 13,466) in the middle of the FS PNA sequence were changed to cytosine residues, formed a complex at a ratio of 1:10. However, the amount of the complex was much less than that formed with the probe and FS PNA at the molar ratio of 1:1 (compare lane 2 with lane 6). Together, these results indicate the sequence-specific, efficient binding of FS PNA to its target in the complex pseudoknot structure of the – PRF signal.

3.2. Sequence-specific inhibition of −1 frameshifting by CPP-conjugated PNA

To evaluate the effect of FS PNA on frameshifting in cell culture, we conjugated FS PNA at the N-terminus to HIV-1 Tat peptide

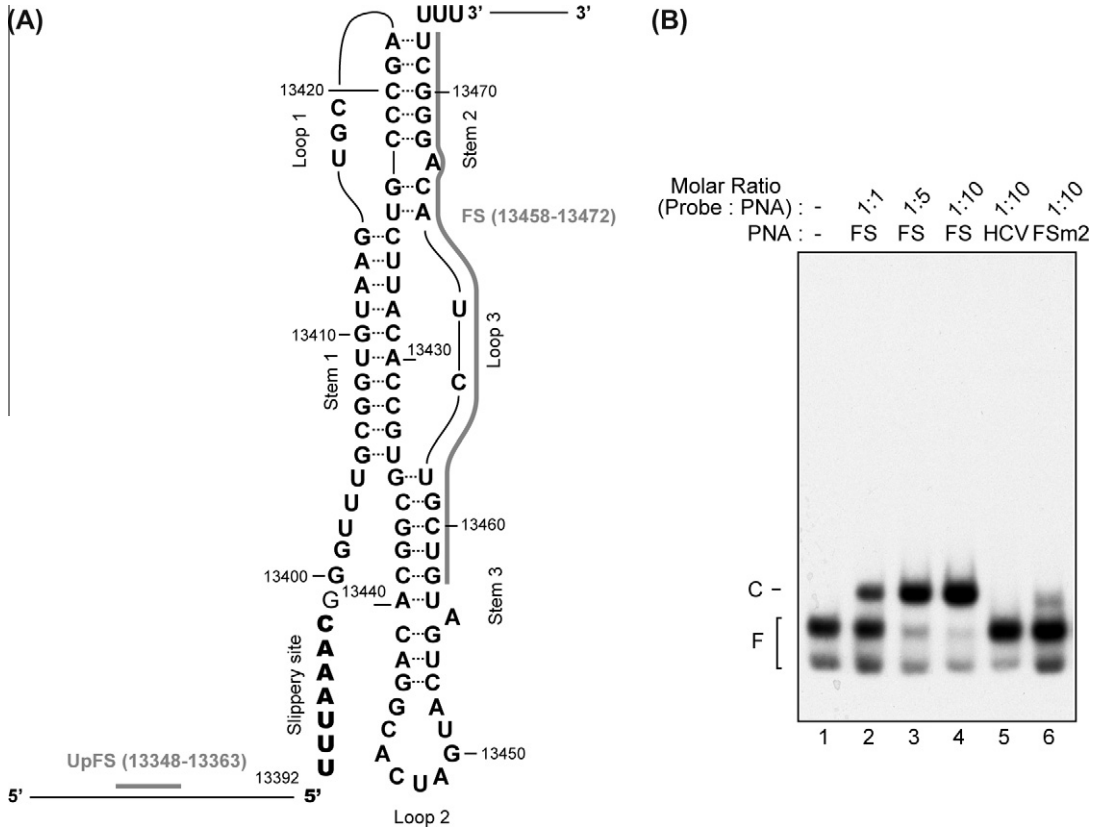

Fig. 1. Secondary structure of programmed −1 ribosomal frameshift signal and specific binding of FS PNA to its target site. (A) PNA target sites are depicted in the secondary structure of −1 PRF signal by thick lines. PNAs were designed to be complementary to the target sites. (B) The 5′-end ^{32}P-labeled RNA probe (10 fmol) was incubated with FS PNA, FSm2 PNA, or HCV PNA in various probe–PNA molar ratios. The mixtures were resolved on a 5% non-denaturing polyacrylamide gel. Free probes (F) and probe–PNA complexes (C) are indicated.

Tat_{57-49} (RRRQRRKKR) (Wender et al., 2000), a well known cell-penetrating peptide (CPP), for delivery of PNA directly into cells. The random coil structure of Tat peptide was suggested to be essential for its rapid translocation across the cellular membrane without causing permanent damage to the membrane integrity, as revealed by solid-state NMR studies using artificial anionic lipid bilayers (Su et al., 2010). Indeed, MTT assay results shown in Fig. 2A demonstrate that the resulting Tat-conjugated FS PNA, named Tat-FS PNA, exerted no significant cytotoxicity up to a concentration of 20 μM in Vero cells.

Frameshift assays were performed in Vero cells using bicistronic dual luciferase reporter plasmids, pJD502 and pJD464 (Plant et al., 2005). In the pJD502 reporter plasmid, −1 PRF signal is located between *Renilla* and firefly luciferase reporters, and the firefly luciferase reporter expression is programmed for translation by ribosomal slippage at the −1 PRF signal (Fig. 2B, top panel). The pJD464 reporter plasmid, in which the −1 PRF signal is inactivated such that the ORF of firefly luciferase is placed in frame with that of *Renilla* luciferase, was used as a zero-frame control plasmid. Vero cells were pre-treated with various concentrations of PNAs and subsequently transfected with pJD464 or pJD502 plasmid to test whether CPP-PNAs inhibits −1 PRF. As shown in Fig. 2B, −1 frameshifting was inhibited in a dose-dependent manner by Tat-FS PNA. An approximately 94% reduction of frameshift efficiency was observed at 5 μM, whereas a non-specific PNA Tat-UpFS, designed to target the region not present in the −1 PRF signal, did not inhibit −1 frameshifting. Furthermore, Tat-FSm2 PNA, carrying two mismatched sequences to the target compared to FS PNA, was less effective in inhibiting −1 frameshifting than Tat-FS PNA. Consistent with the EMSA results shown in Fig. 1B, Tat-HCV PNA displayed no inhibitory effect (Fig. 2C). These results demonstrate that Tat-FS PNA inhibits −1 frameshifting by specifically targeting the pseudoknot structure in −1 PRF signal.

3.3. SARS-CoV replicons expressing a luciferase reporter gene

A SARS-CoV replicon that does not produce infectious virions but still replicates in cells was previously developed for practical, experimental studies of SARS-CoV replication (Almazan et al., 2006). However, replicons allowing convenient, quantitative assays for viral genome replication have not yet been developed. In the present study, we constructed a SARS-CoV replicon that expresses a luciferase reporter gene, using the previous SARS-CoV replicon pBAC-SARS-CoV-REP (Almazan et al., 2006) as a backbone vector, for the sensitive, quantitative detection of viral genome and for cell-based analysis of the antiviral activity of FS PNA. First, the Feo gene (a firefly luciferase gene fused to a neomycin phosphotransferase gene) was amplified from the HCV replicon plasmid pRep-Feo (Tanabe et al., 2004) and linked to cDNA of TRS9, a *cis*-acting RNA element required for sg-mRNA of SARS-CoV. The fused DNA fragment was inserted between the replicase gene (ORF 1a and 1b) and the N gene in pBAC-SARS-CoV-REP (Almazan et al., 2006). The resulting pSARS-REP-Feo plasmid (Fig. 3A, Feo) is expected to produce a viral genome lacking the genes encoding structural proteins, except the N protein, from the cytomegalovirus (CMV) promoter at the 5′-end of the cloned viral cDNA, in transfected cells. In addition, sg-mRNA harboring the Feo gene is expected to be synthesized from the TRS9 preceding the Feo gene by a discontinuous mechanism (Moreno et al., 2008) to display luciferase activity. We also constructed pSARS-REP-ΔTRSFeo, in which a cDNA representing 16-nt TRS9 sequence (5′-AAUAAACGAACAAAUU-3′) preceding the Feo gene was deleted, to prevent the synthesis of sg-mRNAs harboring the Feo gene. Luciferase activity is unlikely to be detected in cells transfected with this plasmid, unless internal initiation of translation, read-through of ribosome complex, or aberrant, non-TRS-mediated generation of sg-mRNAs containing the Feo gene occurs. Finally, another replicon plasmid, pSARS-REP-Feo-MluIrev, in which ORF1a and ORF1b encoding the replicase proteins were altered by inserting the *Mlu*I-digested DNA fragment from the replicase genes into the same vector in the reverse orientation, was also constructed and used as a negative control plasmid.

Using the replicon constructs described above, we first assessed the levels of SARS-CoV replication in BHK21 cells transfected with each of the constructs (pBAC-SARS-CoV-REP, pSARS-REP-Feo, pSARS-REP-ΔTRSFeo, and pSARS-REP-Feo-MluIrev). During replication of SARS-CoV, N sg-mRNA is generated through discontinuous sg-RNA synthesis by the replicase, including the RdRp (nsp12) (Moreno et al., 2008; Pasternak et al., 2001; Thiel et al., 2003). When the minus-strand viral RNA being synthesized reaches TRS9 (Fig. 3A), located upstream of the N-gene, the TRS triggers the minus-strand to jump to the leader TRS (TRS-L depicted in Fig. 3A) sequence, located at the 5′-UTR of the SARS-CoV genome, to complete the synthesis of the rest of the leader sequence. Therefore, the copy number of N gene-specific sg-mRNAs (N sg-mRNA) synthesized during the viral genome replication represents the level of SARS-CoV replication. At 30 h post-transfection, total RNAs were isolated from the cells and N sg-mRNA levels were determined by real-time qRT-PCR. As shown in Fig. 3b, BHK21 cells transfected with

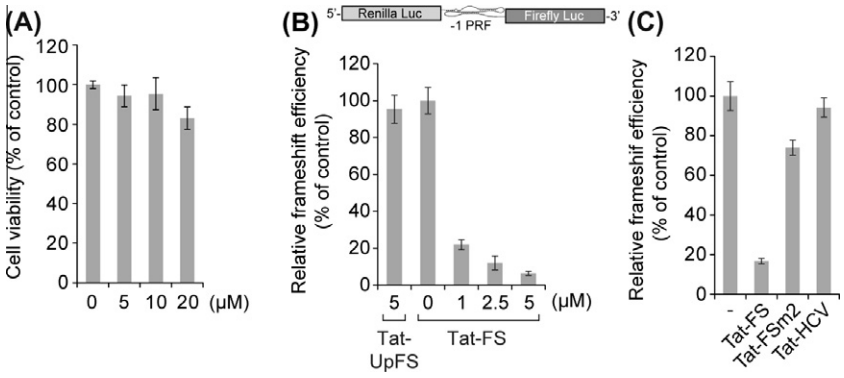

Fig. 2. Inhibition of −1 PRF by CPP-PNA in a cell-based assay. (A) The cytotoxicity of FS PNA in Vero cells was evaluated by the MTT reduction method. Data are expressed as percentages of cell viability in the untreated cells. (B) Vero cells treated with various concentrations of Tat-UpFS or Tat-FS PNAs were transfected with a reporter plasmid harboring the −1 PRF signal (pJD502; upper panel) for measuring frameshifting efficiency, or its derivative, pJD464, which was used as a zero-frame control plasmid. Reporter plasmids were transfected into the cells using DMRIE-C transfection reagent. At 24 h post-transfection, cells were harvested and the ribosomal frameshifting assay was performed. Data are expressed as percentages of normalized firefly luciferase activity in mock-treated cells. (C) Sequence-specific inhibition of frameshifting of PNAs were assessed as in (B) with 5 μM of each indicated PNA. Reporter plasmids were transfected into the cells using Fugene 6. All data in (A–C) represent means ± SD of triplicate measurements from three independent experiments.

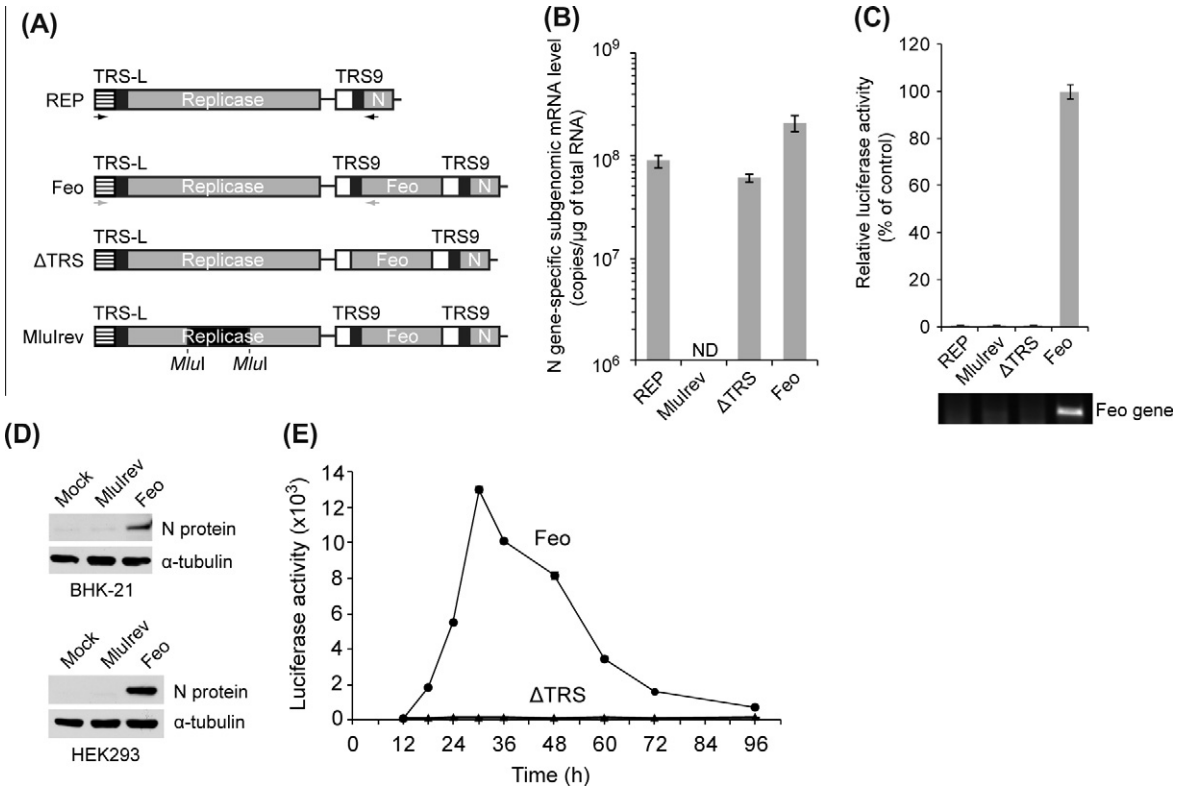

Fig. 3. A SARS-CoV replicon expressing a luciferase reporter. (A) The Feo gene fused or non-fused to TRS9 was inserted into pBAC-SARS-CoV-REP (REP) to construct pSARS-CoV-REP-Feo (Feo) or pSARS-CoV-REP-ΔTRSFeo (ΔTRS), respectively. The pSARS-CoV-REP-Feo-MluIrev (MluIrev), which is defective in synthesis of functional replicase proteins, was used as a negative control plasmid. TRSs are indicated by a black box and leader sequences by a box with deviant crease lines. Black arrows indicate primers used for detection of N gene-specific sg-mRNAs and gray arrows for detection of sg-mRNAs containing the Feo gene. (B and C) BHK-21 cells were co-transfected with replicon plasmids and pRL-TK used for normalization of transfection efficiency, by electroporation. At 30 h post-transfection, cells were harvested and analyzed for sg-mRNA level, luciferase activity, and intracellular SARS-CoV nucleocapsid N protein level. (B) The N gene-specific sg-mRNA level was quantified by real-time qRT-PCR using a TaqMan probe. Subgenomic RNA copy numbers per μg total RNA are shown. ND, not detected. (C) Firefly luciferase activity from the replicon plasmid was normalized to *Renilla* luciferase activity from the pRL-TK plasmid. Normalized luciferase activity of cells transfected with pSARS-CoV-REP was defined as 100. Endogenous sg-mRNAs containing Feo gene was amplified by RT-PCR and resulting PCR products were resolved by agarose gel electrophoresis (low panel). (D) BHK-21 or HEK293 cells were left untransfected (Mock) or transfected with the plasmid indicated above the blots. N protein and α-tubulin were detected by Western blot analysis. (E) Kinetics of SARS-CoV replicon replication in transiently transfected cells. BHK-21 cells were transfected with pSARS-REP-Feo (●) or pSARS-REP-ΔTRSFeo (▲) by electroporation. Cells were harvested at each given time point and store at −80 °C until analysis. Luciferase activity was measured with the same amount of cell lysate. Data from one representative experiment from two independent experiments with similar results are shown.

each of the replicon plasmids, pBAC-SARS-CoV-REP, pSARS-REP-Feo, or pSARS-REP-ΔTRSFeo produced a similar level of sg-mRNAs (6×10^7–2×10^8 genome copies/μg of total RNA), whereas pSARS-REP-Feo-MluIrev was found defective in the generation of sg-mRNAs.

We could detect a high level of luciferase activity only in the cells transfected with pSARS-REP-Feo plasmid (Fig. 3C). In addition, synthesis of sg-mRNAs containing Feo gene was confirmed by detection of 300-bp Feo gene-specific RT-PCR-amplified products (bottom panel). The luciferase activity in the cells transfected with a control plasmid, pSARS-REP-ΔTRSFeo, which lacks the TRS9 fused to the Feo gene and thereby is expected to fail to yield sg-mRNAs for the Feo gene, remained at background levels. Consistent with the luciferase activity assay results, we did not detect sg-mRNA containing the Feo gene in cells transfected with pSARS-REP-ΔTRSFeo, even though this replicon plasmid was able to generate sg-mRNA for the N-gene, as shown in Fig. 3B. As expected, neither N gene-specific sg-mRNA nor Feo gene-specific sg-mRNA was generated from pSARS-REP-Feo-MluIrev. As shown in Fig. 3D, we used Western blot analysis to confirm the expression of N protein in two different cell lines, BHK-21 and HEK293, which are known to support SARS-CoV replication (Almazan et al., 2006; Kaye, 2006) upon transfection with the pSARS-REP-Feo plasmid. In contrast, replication-defective pSARS-REP-Feo-MluIrev did not lead to accumulation of the N protein.

We next analyzed the kinetics of the SARS-CoV replicon replication by measuring luciferase activities in cell lysates prepared from BHK-21 cells transfected with pSARS-REP-Feo or pSARS-REP-ΔTRS-Feo, at different time points post-transfection, up to 96 h. In the cells transfected with pSARS-REP-Feo, the luciferase activity reached the highest level at 30 h post-transfection and the detectable level of activity persisted for up to 96 h (Fig. 3E). In contrast, the cells transfected with pSARS-REP-ΔTRSFeo showed a basal level of luciferase activity and the activity did not increase within 96 h. These results indicate that the luciferase activity was derived from the Feo gene-containing sg-mRNAs, whose synthesis is regulated by the TRS9 located upstream of the Feo gene in the pSARS-REP-Feo replicon plasmid.

3.4. Suppression of SARS-CoV replication in SARS-CoV replicon cells by Tat-FS PNA

Inhibition of the ribosomal frameshifting by disruption of the −1 PRF signal pseudoknot structure would decrease the intracellular level of replicase proteins encoded by ORF1b and thereby affect viral genome replication. Having developed the SARS-CoV replicon, we evaluated the antiviral activity of Tat-FS PNA in HEK293 cells transiently transfected with pSARS-REP-Feo replicon plasmid. As shown in Fig. 4A, 10 μM Tat-FS PNA inhibited viral replication by 82%, whereas Tat-conjugated J3U2 PNA targeting the 3′-UTR of

Japanese encephalitis virus (JEV) genome did not affect the viral replication at the same concentration. Consistent with the EMSA and frameshifting reporter assay results shown in Figs. 1B and 2C, respectively, the two-nucleotide mismatched PNA Tat-FSm2 showed a dramatically reduced antiviral activity. These results together clearly demonstrated sequence-specific inhibition of −1 PRF by Tat-FS PNA. In comparison, IFN-β 1a, a potent interferon in reducing SARS-CoV replication *in vitro* (Cinatl et al., 2003), reduced the luciferase activity by 46% when the replicon-replicating cells were treated with 250 IU/ml IFN-β Synthetic double-stranded RNA Poly(I:C), which triggers type I IFN (α/β) production (Kato et al., 2006), also led to suppression of SARS-CoV replication. Tat-FS PNA suppressed SARS-CoV replication in a dose-dependent manner, with an IC_{50} value of 4.4 μM (Fig. 4B).

As PNAs are nucleic acids with an unusual backbone structure, it is possible that PNAs are recognized by cytosolic nucleic acid-recognition receptor proteins such as retinoic acid inducible gene I (RIG-I) and melanoma differentiation factor 5 (MDA5) involved in innate immune responses (Kawai and Akira, 2006; Meylan and Tschopp, 2006), and induce IFN-β expression that can lead to inhibition of viral replication. To confirm that the inhibition of viral replication by PNA was not due to IFN responses activated by PNA, we wondered whether there was an induction of IFN-β expression in HEK293 cells treated with 10 μM Tat-FS PNA. As shown in Fig. 4C, Tat-conjugated FS PNA, as well as Tat-FSm2, had no potent impact on the induction of IFN-β responses, while the luciferase activity driven by IFN-β promoter activation increased by 225-fold in cells transfected with a plasmid expressing the active form of IRF3. Two RNA molecules, poly(I:C) and HCV 3′-UTR, which are known to be recognized by MDA5 and RIG-I, respectively and induce type I IFN production (Kato et al., 2008; Pichlmair et al., 2006; Saito et al., 2008), also induced IFN-β promoter activation under the same experimental conditions. Furthermore, qRT-PCR analysis showed that neither Tat-FS nor Tat-FSm2 resulted in a transcriptional upregulation of IFN-β gene as well as an IFN-stimulated gene ISG56, thus confirming our result with the reporter system. Altogether, these results indicate that inhibition of SARS-CoV replication by Tat-FS PNA was not due to indirect effects caused by induction of IFN-β expression in cell culture.

4. Discussion

cis-Acting RNA elements of RNA viruses, such as the untranslated regions of viral genomes, are well-conserved in sequence and structure and have been chosen for targets of antiviral thera-

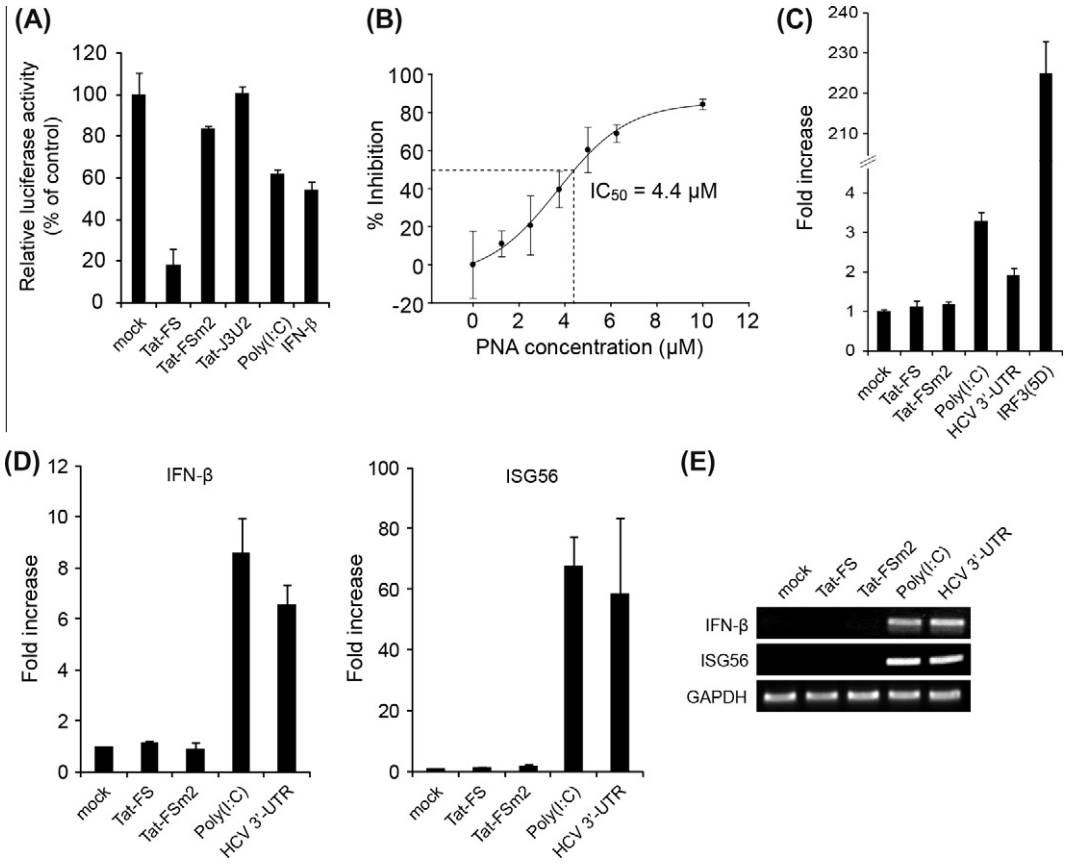

Fig. 4. Suppression of SARS-CoV replication by Tat-peptide-conjugated FS PNA in SARS-CoV replicon-replicating cells. (A) HEK293 cells, co-transfected with pSARS-REP-Feo and pRL-TK, were treated with each indicated PNA (10 μM) in serum-free DMEM for 3 h at 6 h post-transfection. Tat-conjugated J3U2 PNA (Tat-J3U2) targeting the 3′-UTR of JEV genome was used as a negative control. IFN-β (250 IU/ml) and IFN-β inducer poly(I:C) (0.8 μg/ml) were used as positive controls. Poly(I:C) was transfected into the cells using lipofectamin RNAiMAX agent. After 30 h incubation in complete medium, cells were harvested and luciferase activity was measured. (B) The IC_{50} value for the inhibition of SARS-CoV replication by Tat-FS PNA was determined at various PNA concentrations. (C) HEK293 cells were co-transfected with IFNβ-pGL3 luciferase reporter plasmid and pRL-TK used for normalization of transfection efficiency, prior to mock-treatment or treatment with 10 μM of Tat-FS or Tat-FSm2 PNA. Poly(I:C) or HCV 3′-UTR at a final concentration of 2 μg/ml or expression of an active form of IRF3, IRF3(5D) was used as a positive control for stimulation of IFN-β promoter activity. The normalized firefly luciferase activity of the mock-treated cells is considered one unit and the increase in luciferase activity is shown as fold induction. (D) HEK293 cells treated with PNAs or indicated RNAs as in (C) were analyzed for IFN-β and ISG56 mRNA abundance by real-time qRT-PCR. Fold increase in mRNA abundance is shown. (E) The real-time PCR products representing the abundance of the indicated mRNAs were visualized by agarose gel electrophoresis and ethidium bromide staining. Detection of GAPDH mRNA served as control. Results are from a representative experiment of $n = 3$ that gave similar results. (A–D) Data represent means ± SD of triplicate measurements from three independent experiments.

pies using antisense oligonucleotides (Deas et al., 2005; Neuman et al., 2006; Tallet-Lopez et al., 2003; Yoo et al., 2009). In the present study, we designed an antisense PNA targeting a selected region of the pseudoknot structure in the SARS-CoV −1 PRF signal and evaluated its effects on frameshifting and viral RNA replication. We demonstrated that the FS PNA targeting stems 2 and 3 effectively down-regulates SARS-CoV replication by interfering with −1 frameshifting. Sequence-specific inhibition of −1 PRF by FS PNA was demonstrated in cell-based assays, using bicistronic frameshift assay reporter plasmids. Our results are consistent with the previous findings showing, by mutational analysis, that the specific sequences and structures of stems 2 and 3 in the pseudoknot structure are important for frameshifting (Plant et al., 2005). A series of mutations disrupting stem 2 was shown to lead to a dramatic reduction of frameshifting (Baranov et al., 2005; Plant et al., 2005; Su et al., 2005). Moreover, we have demonstrated that the pseudoknot structure of SARS-CoV is a critical stimulatory component of the −1 PRF signal required for viral replication. The FS PNA effectively reduced frameshifting, suppressing viral replication with an IC_{50} value of 4.4 μM, in cell culture.

RNA viruses often spontaneously generate mutants resistant to antiviral drugs due to low fidelity of their RNA polymerases. However, alignment analysis of the −1 PRF signals from over 130 different strains of SARS-CoV showed that the target of the PNA used in this study is extremely conserved in sequence. Therefore, there is a good possibility that emerging FS PNA-resistant mutants will have to pay a significant cost in decreased −1 PRF, leading to a decreased level of viral replicase proteins encoded by the ORF1b downstream of the −1 PRF signal. Our results collectively underscore that the conserved pseudoknot sequence targeted by antisense FS PNA is a crucial druggable target, particularly in view of the importance of the maintenance of stoichiometry between nonstructural proteins encoded by ORF1a and 1b for SASR-CoV replication (Plant et al., 2010).

Ribosomal pausing caused by the presence of stable RNA structures such as pseudoknots has been proposed to be an initial step driving −1 PRF (Namy et al., 2006). Consistent with this notion, prior studies have demonstrated that antisense oligonucleotides, including morpholino oligonucleotides, designed to anneal to mRNA downstream of the slippery-site, induce ribosome frameshifting in an *in vitro* translation system using rabbit reticulocyte lysates (Howard et al., 2004; Olsthoorn et al., 2004; Yu et al., 2010). Contrary to previous reports, our results demonstrate that the antisense FS PNA, which targets the 3′-end region of the SARS-CoV pseudoknot structure, including stem 2, loop 3, and part of stem 3, impedes frameshifting. Binding of PNA, which has high hybridization ability due to its flexible, neutral backbone (Hanvey et al., 1992; Nielsen et al., 1991), to this target might lead to disruption of stable structures in stems 2 and 3 through the formation of an RNA–PNA hybrid duplex structure. The resulting hybrid molecules would probably be more stable due to less electrostatic repulsion forces between PNA and RNA molecules than the RNA–RNA base-paring present in the parental pseudoknot structure. Consequently, the RNA structures upstream of this PNA-binding site might form an alternative secondary structure for ribosomes to elongate without pausing and thus interfere with frameshifting. Alternatively, as long as the stem1 structure remains intact, ribosomal shifting may still occur. Supporting this hypothesis, previous studies have shown that the stable stem-structure at the bottom of the stem 1 plays an important role in efficient frameshifting (Baranov et al., 2005), since the structure hampers elongation of peptides by acting as a barrier for the ribosome-associated helicase (Namy et al., 2004). Even if −1 PRF occurs by the preserved stem 1 structure, the stable PNA–RNA structures upstream of stem 1 would hinder the ribosome elongation, resulting in suppression of the translation of downstream genes. It is also possible that a PNA–RNA hybrid structure downstream of the slip-site, *per se*, forces the paused ribosomes to situate over the incorrect frameshift sequence. In summary, alterations in RNA secondary structure, either at the PNA-annealing site and/or an upstream region, which could be caused by PNA hybridization to stems 2 and 3, along with loop 3, appears to contribute to the suppression of frameshifting. Whatever the mechanism, such changes in the pseudoknot structure may alter a specific kinetic barrier to ribosome translocation, playing a role in the fine modulation of frameshifting. Indeed, previous studies have consistently revealed that the extent of pausing of ribosomes does not appear to be a sufficient determinant for efficient frameshifting (Kontos et al., 2001). The conformational feature of the pseudoknot, but not simply the ribosome stalling caused by a stacked stable stem structure, has been suggested to be critical for the promotion of frameshifting (Somogyi et al., 1993). Finally, the pseudoknot-targeting PNA might interfere with the interaction between the −1 PRF signal and viral and/or cellular protein, if any. It is currently unknown whether cellular proteins are involved in frameshifting by binding to the −1 PRF signal or whether SARS-CoV-encoded proteins participate in negative or positive regulation of frameshifting during the infection cycle.

IFNs are broad antiviral agents together with ribavirin. In cell-based *in vitro* assays, IFN-β shows the most potent inhibitory effect against SARS-CoV among IFN-α, β, and γ when tested in virus-infected Vero E6 cells (Cinatl et al., 2003; Hensley et al., 2004). We confirmed the anti-SARS-CoV activity of IFN-β; treatment with 250 IU/ml human IFN-β 1a led to 46% inhibition of SARS-CoV replication in our replicon system (Fig. 4A). We also found that Tat-conjugated PNA is not a potent innate immune response stimulator, leading to induction of IFN-β expression. We observed neither a decrease in viral replication with a control Tat-conjugated PNA nor induction of IFN-β response by FS-PNA. We conclude that the suppression of SARS-CoV replication was primarily mediated by inhibition of frameshifting by FS-PNA. However, it is possible that CPP-PNA or PNA itself binds to known or not-yet-defined extracellular or intracellular receptors of immune cells to induce unexpected immune responses *in vivo*. It has been reported that PNA stimulates IFN-γ in peripheral blood mononuclear cell cultures and inhibits the replication of HIV (Hirschman and Chen, 1996). Whether Tat-conjugated PNA mediates its antiviral effect through IFN-γ awaits *in vivo* experiments, although SARS-CoV replication is not effectively controlled by IFN-γ at least in cell culture (Cinatl et al., 2003). An evaluation of the *in vivo* efficacy of PNA is needed to clarify the immune response induction issues.

In summary, our results confirm predictions from the recent literature suggesting that the −1 PRF signal is essential for SARS-CoV replication (Plant et al., 2010). Further, we show that the CPP–PNA can access the complex −1 PRF pseudoknot structure to interfere with −1 frameshifting, leading to inhibition of SARS-CoV replication. It is fully expected that CPP-PNAs targeting −1 PRF signal of other pathogenic RNA viruses will have similar antiviral activity. We also established a SARS-CoV replicon system enabling the high-throughput screening of antivirals. The system proved to be a robust replication assay tool when applied to the evaluation of antiviral activities of PNAs. Using this replicon, we demonstrated for the first time that CPP-PNAs targeting the −1 PRF have potential as an anti-viral reagent against SARS-CoV.

Acknowledgements

We thank Dr. John Hiscott (McGill University, Montreal, Quebec, Canada) for providing the IFNβ-pGL3 luciferase reporter and a vector expressing an active form of IRF, and Dr. Naoya Sakamoto (Tokyo Medical and Dental University, Tokyo, Japan) for providing the pRep-Feo plasmid. This work was supported by

a grant from the Seoul R&BD Program (Grant 10580) and a grant from Translation Research Center for Protein Function Control funded by the National Research Foundation of Korea (NRF-2009-0092959). D.G.A., W.L., and J.K.C. were supported in part by the BK21 program of the Korean Ministry of Education, Science, and Technology.

References

Almazan, F., Dediego, M.L., Galan, C., Escors, D., Alvarez, E., Ortego, J., Sola, I., Zuniga, S., Alonso, S., Moreno, J.L., Nogales, A., Capiscol, C., Enjuanes, L., 2006. Construction of a severe acute respiratory syndrome coronavirus infectious cDNA clone and a replicon to study coronavirus RNA synthesis. J. Virol. 80, 10900–10906.

Baranov, P.V., Gesteland, R.F., Atkins, J.F., 2002. Recoding: translational bifurcations in gene expression. Gene 286, 187–201.

Baranov, P.V., Henderson, C.M., Anderson, C.B., Gesteland, R.F., Atkins, J.F., Howard, M.T., 2005. Programmed ribosomal frameshifting in decoding the SARS-CoV genome. Virology 332, 498–510.

Brierley, I., Digard, P., Inglis, S.C., 1989. Characterization of an efficient coronavirus ribosomal frameshifting signal: requirement for an RNA pseudoknot. Cell 57, 537–547.

Cinatl Jr., J., Michaelis, M., Hoever, G., Preiser, W., Doerr, H.W., 2005. Development of antiviral therapy for severe acute respiratory syndrome. Antiviral Res. 66, 81–97.

Cinatl, J., Morgenstern, B., Bauer, G., Chandra, P., Rabenau, H., Doerr, H.W., 2003. Treatment of SARS with human interferons. Lancet 362, 293–294.

Deas, T.S., Binduga-Gajewska, I., Tilgner, M., Ren, P., Stein, D.A., Moulton, H.M., Iversen, P.L., Kauffman, E.B., Kramer, L.D., Shi, P.Y., 2005. Inhibition of flavivirus infections by antisense oligomers specifically suppressing viral translation and RNA replication. J. Virol. 79, 4599–4609.

Hanvey, J.C., Peffer, N.J., Bisi, J.E., Thomson, S.A., Cadilla, R., Josey, J.A., Ricca, D.J., Hassman, C.F., Bonham, M.A., Au, K.G., et al., 1992. Antisense and antigene properties of peptide nucleic acids. Science 258, 1481–1485.

Hensley, L.E., Fritz, L.E., Jahrling, P.B., Karp, C.L., Huggins, J.W., Geisbert, T.W., 2004. Interferon-beta 1a and SARS coronavirus replication. Emerg. Infect. Dis. 10, 317–319.

Hirschman, S.Z., Chen, C.W., 1996. Peptide nucleic acids stimulate gamma interferon and inhibit the replication of the human immunodeficiency virus. J. Investig. Med. 44, 347–351.

Howard, M.T., Gesteland, R.F., Atkins, J.F., 2004. Efficient stimulation of site-specific ribosome frameshifting by antisense oligonucleotides. RNA 10, 1653–1661.

Kato, H., Takeuchi, O., Mikamo-Satoh, E., Hirai, R., Kawai, T., Matsushita, K., Hiiragi, A., Dermody, T.S., Fujita, T., Akira, S., 2008. Length-dependent recognition of double-stranded ribonucleic acids by retinoic acid-inducible gene-I and melanoma differentiation-associated gene 5. J. Exp. Med. 205, 1601–1610.

Kato, H., Takeuchi, O., Sato, S., Yoneyama, M., Yamamoto, M., Matsui, K., Uematsu, S., Jung, A., Kawai, T., Ishii, K.J., Yamaguchi, O., Otsu, K., Tsujimura, T., Koh, C.S., Reis e Sousa, C., Matsuura, Y., Fujita, T., Akira, S., 2006. Differential roles of MDA5 and RIG-I helicases in the recognition of RNA viruses. Nature 441, 101–105.

Kawai, T., Akira, S., 2006. Innate immune recognition of viral infection. Nat. Immunol. 7, 131–137.

Kaye, M., 2006. SARS-associated coronavirus replication in cell lines. Emerg. Infect. Dis. 12, 128–133.

Kim, S.J., Kim, J.H., Kim, Y.G., Lim, H.S., Oh, J.W., 2004. Protein kinase C-related kinase 2 regulates hepatitis C virus RNA polymerase function by phosphorylation. J. Biol. Chem. 279, 50031–50041.

Kontos, H., Napthine, S., Brierley, I., 2001. Ribosomal pausing at a frameshifter RNA pseudoknot is sensitive to reading phase but shows little correlation with frameshift efficiency. Mol. Cell. Biol. 21, 8657–8670.

Li, K., Chen, Z., Kato, N., Gale Jr., M., Lemon, S.M., 2005. Distinct poly(I-C) and virus-activated signaling pathways leading to interferon-beta production in hepatocytes. J. Biol. Chem. 280, 16739–16747.

Lin, R., Genin, P., Mamane, Y., Hiscott, J., 2000. Selective DNA binding and association with the CREB binding protein coactivator contribute to differential activation of alpha/beta interferon genes by interferon regulatory factors 3 and 7. Mol. Cell. Biol. 20, 6342–6353.

Marra, M.A., Jones, S.J., Astell, C.R., Holt, R.A., Brooks-Wilson, A., Butterfield, Y.S., Khattra, J., Asano, J.K., Barber, S.A., Chan, S.Y., Cloutier, A., Coughlin, S.M., Freeman, D., Girn, N., Griffith, O.L., Leach, S.R., Mayo, M., McDonald, H., Montgomery, S.B., Pandoh, P.K., Petrescu, A.S., Robertson, A.G., Schein, J.E., Siddiqui, A., Smailus, D.E., Stott, J.M., Yang, G.S., Plummer, F., Andonov, A., Artsob, H., Bastien, N., Bernard, K., Booth, T.F., Bowness, D., Czub, M., Drebot, M., Fernando, L., Flick, R., Garbutt, M., Gray, M., Grolla, A., Jones, S., Feldmann, H., Meyers, A., Kabani, A., Li, Y., Normand, S., Stroher, U., Tipples, G.A., Tyler, S., Vogrig, R., Ward, D., Watson, B., Brunham, R.C., Krajden, M., Petric, M., Skowronski, D.M., Upton, C., Roper, R.L., 2003. The genome sequence of the SARS-associated coronavirus. Science 300, 1399–1404.

Masters, P.S., 2006. The molecular biology of coronaviruses. Adv. Virus Res. 66, 193–292.

McCormick, C.J., Challinor, L., Macdonald, A., Rowlands, D.J., Harris, M., 2004. Introduction of replication-competent hepatitis C virus transcripts using a tetracycline-regulable baculovirus delivery system. J. Gen. Virol. 85, 429–439.

Meylan, E., Tschopp, J., 2006. Toll-like receptors and RNA helicases: two parallel ways to trigger antiviral responses. Mol. Cell 22, 561–569.

Moreno, J.L., Zuniga, S., Enjuanes, L., Sola, I., 2008. Identification of a coronavirus transcription enhancer. J. Virol. 82, 3882–3893.

Namy, O., Moran, S.J., Stuart, D.I., Gilbert, R.J., Brierley, I., 2006. A mechanical explanation of RNA pseudoknot function in programmed ribosomal frameshifting. Nature 441, 244–247.

Namy, O., Rousset, J.P., Napthine, S., Brierley, I., 2004. Reprogrammed genetic decoding in cellular gene expression. Mol. Cell 13, 157–168.

Neuman, B.W., Stein, D.A., Kroeker, A.D., Moulton, H.M., Bestwick, R.K., Iversen, P.L., Buchmeier, M.J., 2006. Inhibition and escape of SARS-CoV treated with antisense morpholino oligomers. Adv. Exp. Med. Biol. 581, 567–571.

Nielsen, P.E., 2010. Peptide nucleic acids (PNA) in chemical biology and drug discovery. Chem. Biodivers. 7, 786–804.

Nielsen, P.E., Egholm, M., Berg, R.H., Buchardt, O., 1991. Sequence-selective recognition of DNA by strand displacement with a thymine-substituted polyamide. Science 254, 1497–1500.

Oh, J.W., Ito, T., Lai, M.M., 1999. A recombinant hepatitis C virus RNA-dependent RNA polymerase capable of copying the full-length viral RNA. J. Virol. 73, 7694–7702.

Olsthoorn, R.C., Laurs, M., Sohet, F., Hilbers, C.W., Heus, H.A., Pleij, C.W., 2004. Novel application of sRNA: stimulation of ribosomal frameshifting. RNA 10, 1702–1703.

Pasternak, A.O., van den Born, E., Spaan, W.J., Snijder, E.J., 2001. Sequence requirements for RNA strand transfer during nidovirus discontinuous subgenomic RNA synthesis. EMBO J. 20, 7220–7228.

Peiris, J.S., Guan, Y., Yuen, K.Y., 2004. Severe acute respiratory syndrome. Nat. Med. 10, S88–S97.

Pichlmair, A., Schulz, O., Tan, C.P., Naslund, T.I., Liljestrom, P., Weber, F., Reis e Sousa, C., 2006. RIG-I-mediated antiviral responses to single-stranded RNA bearing 5′-phosphates. Science 314, 997–1001.

Plant, E.P., Perez-Alvarado, G.C., Jacobs, J.L., Mukhopadhyay, B., Hennig, M., Dinman, J.D., 2005. A three-stemmed mRNA pseudoknot in the SARS coronavirus frameshift signal. PLoS Biol. 3, e172.

Plant, E.P., Rakauskaite, R., Taylor, D.R., Dinman, J.D., 2010. Achieving a golden mean: mechanisms by which coronaviruses ensure synthesis of the correct stoichiometric ratios of viral proteins. J. Virol. 84, 4330–4340.

Prentice, E., McAuliffe, J., Lu, X., Subbarao, K., Denison, M.R., 2004. Identification and characterization of severe acute respiratory syndrome coronavirus replicase proteins. J. Virol. 78, 9977–9986.

Rota, P.A., Oberste, M.S., Monroe, S.S., Nix, W.A., Campagnoli, R., Icenogle, J.P., Penaranda, S., Bankamp, B., Maher, K., Chen, M.H., Tong, S., Tamin, A., Lowe, L., Frace, M., DeRisi, J.L., Chen, Q., Wang, D., Erdman, D.D., Peret, T.C., Burns, C., Ksiazek, T.G., Rollin, P.E., Sanchez, A., Liffick, S., Holloway, B., Limor, J., McCaustland, K., Olsen-Rasmussen, M., Fouchier, R., Gunther, S., Osterhaus, A.D., Drosten, C., Pallansch, M.A., Anderson, L.J., Bellini, W.J., 2003. Characterization of a novel coronavirus associated with severe acute respiratory syndrome. Science 300, 1394–1399.

Saito, T., Owen, D.M., Jiang, F., Marcotrigiano, J., Gale Jr., M., 2008. Innate immunity induced by composition-dependent RIG-I recognition of hepatitis C virus RNA. Nature 454, 523–527.

Schmittgen, T.D., Livak, K.J., 2008. Analyzing real-time PCR data by the comparative C(T) method. Nat. Protoc. 3, 1101–1108.

Snijder, E.J., Bredenbeek, P.J., Dobbe, J.C., Thiel, V., Ziebuhr, J., Poon, L.L., Guan, Y., Rozanov, M., Spaan, W.J., Gorbalenya, A.E., 2003. Unique and conserved features of genome and proteome of SARS-coronavirus, an early split-off from the coronavirus group 2 lineage. J. Mol. Biol. 331, 991–1004.

Sola, I., Moreno, J.L., Zuniga, S., Alonso, S., Enjuanes, L., 2005. Role of nucleotides immediately flanking the transcription-regulating sequence core in coronavirus subgenomic mRNA synthesis. J. Virol. 79, 2506–2516.

Somogyi, P., Jenner, A.J., Brierley, I., Inglis, S.C., 1993. Ribosomal pausing during translation of an RNA pseudoknot. Mol. Cell. Biol. 13, 6931–6940.

Su, M.C., Chang, C.T., Chu, C.H., Tsai, C.H., Chang, K.Y., 2005. An atypical RNA pseudoknot stimulator and an upstream attenuation signal for −1 ribosomal frameshifting of SARS coronavirus. Nucleic Acids Res. 33, 4265–4275.

Su, Y., Waring, A.J., Ruchala, P., Hong, M., 2010. Membrane-bound dynamic structure of an arginine-rich cell-penetrating peptide, the protein transduction domain of HIV TAT, from solid-state NMR. Biochemistry 49, 6009–6020.

Tallet-Lopez, B., Aldaz-Carroll, L., Chabas, S., Dausse, E., Staedel, C., Toulme, J.J., 2003. Antisense oligonucleotides targeted to the domain IIId of the hepatitis C virus IRES compete with 40S ribosomal subunit binding and prevent in vitro translation. Nucleic Acids Res. 31, 734–742.

Tanabe, Y., Sakamoto, N., Enomoto, N., Kurosaki, M., Ueda, E., Maekawa, S., Yamashiro, T., Nakagawa, M., Chen, C.H., Kanazawa, N., Kakinuma, S., Watanabe, M., 2004. Synergistic inhibition of intracellular hepatitis C virus replication by combination of ribavirin and interferon-alpha. J. Infect. Dis. 189, 1129–1139.

te Velthuis, A.J., Arnold, J.J., Cameron, C.E., van den Worm, S.H., Snijder, E.J., 2010. The RNA polymerase activity of SARS-coronavirus nsp12 is primer dependent. Nucleic Acids Res. 38, 203–214.

Thiel, V., Ivanov, K.A., Putics, A., Hertzig, T., Schelle, B., Bayer, S., Weissbrich, B., Snijder, E.J., Rabenau, H., Doerr, H.W., Gorbalenya, A.E., Ziebuhr, J., 2003. Mechanisms and enzymes involved in SARS coronavirus genome expression. J. Gen. Virol. 84, 2305–2315.

Tong, T.R., 2009. Therapies for coronaviruses. Part I of II – viral entry inhibitors. Expert Opin. Ther. Pat. 19, 357–367.

Wang, L.F., Shi, Z., Zhang, S., Field, H., Daszak, P., Eaton, B.T., 2006. Review of bats and SARS. Emerg. Infect. Dis. 12, 1834–1840.

Wender, P.A., Mitchell, D.J., Pattabiraman, K., Pelkey, E.T., Steinman, L., Rothbard, J.B., 2000. The design, synthesis, and evaluation of molecules that enable or enhance cellular uptake: peptoid molecular transporters. Proc. Natl. Acad. Sci. USA 97, 13003–13008.

Xu, X., Liu, Y., Weiss, S., Arnold, E., Sarafianos, S.G., Ding, J., 2003. Molecular model of SARS coronavirus polymerase: implications for biochemical functions and drug design. Nucleic Acids Res. 31, 7117–7130.

Yoo, J.S., Kim, C.M., Kim, J.H., Kim, J.Y., Oh, J.W., 2009. Inhibition of Japanese encephalitis virus replication by peptide nucleic acids targeting cis-acting elements on the plus- and minus-strands of viral RNA. Antiviral Res. 82, 122–133.

Yu, C.H., Noteborn, M.H., Olsthoorn, R.C., 2010. Stimulation of ribosomal frameshifting by antisense LNA. Nucleic Acids Res. 38, 8277–8283.

Zhu, Q., Guo, J.T., Seeger, C., 2003. Replication of hepatitis C virus subgenomes in nonhepatic epithelial and mouse hepatoma cells. J. Virol. 77, 9204–9210.